IET Electric Power Applications

Research Article

IET Journals
The Institution of Engineering and Technology

Quick and seamless transition method for I-f to sensorless vector control changeover and on-the-fly start of PMSM drives

ISSN 1751-8660
Received on 6th May 2020
Revised 20th June 2020
Accepted on 7th July 2020
E-First on 12th August 2020
doi: 10.1049/iet-epa.2020.0387
www.ietdl.org

Sandeep V. Nair[1] ✉, *Kamalesh Hatua*[1], *N.V.P.R. Durga Prasad*[2], *D. Kishore Reddy*[2]

[1]*Electrical Engineering Department, IIT Madras, Chennai, India*
[2]*BHEL Corp., R&D, Hyderabad, India*
✉ *E-mail: sandeepvnair89@gmail.com*

Abstract: A smooth changeover from the I-f method to closed-loop sensorless vector control is a critical requirement for permanent magnet synchronous motor (PMSM) drives using a back-emf based sensorless algorithm for medium- to high-speed range control. The existing methods provide a smooth transition by aligning the angle generated by I-f control to the sensorless estimated angle. However, the overall start-up time increases due to the additional transition interval, which limits the usability of these methods for applications requiring a quick start-up. Furthermore, the use of a direct transition method to reduce the changeover time results in speed and current oscillation if the estimated position using sensorless algorithm is having an error. In the proposed method, the inverter pulses are disabled for a short duration and the machine back-emf is measured after the stator current falls to zero. Therefore, a quick and seamless transition is achieved in the proposed method by accurately estimating the rotor position from the sensed back-emf. The proposed method is also extended to perform on-the-fly start for power failure ride through during short time power supply interruption. The performance of the proposed method is verified using simulation and experiment on a 25 kW PMSM drive.

1 Introduction

Permanent magnet synchronous motors (PMSMs) are widely used in industries, home appliances, and electric vehicles due to their high energy density, high torque capability at low speed, and higher efficiency than induction machines. Position sensors or resolvers are used conventionally for the vector control of PMSM drives. However, the use of position sensors affects system reliability and increases cost. Consequently, sensorless vector control methods became popular. For a variety of applications such as compressors, pumps, fans, and heating ventilation and air conditioning systems, and also for critical applications such as electric ship propulsion, and emergency heat and smoke exhaust, a high precision dynamic control at low speed is not necessary. Instead, a simple and reliable control in medium- and high-speed range would be sufficient. Hence, back-emf based sensorless vector control is an appropriate choice for such applications. However, the operation of back-emf based methods is limited at zero or very low speeds. Therefore, an additional starting method is necessary while using back-emf based sensorless vector control.

High-frequency signal injection techniques [1–3] can be used for starting and low-speed region. In these methods, the rotor position is extracted from the rotor anisotropy and the saturation saliency of the motor. However, the complex signal processing requirements and implementation difficulties for low-saliency machines limits their application. Hence, an open-loop method for starting along with back-emf based sensorless vector control is commonly used. One such strategy is to use V/f control for starting and low-speed operation [4]. However, since there is no current feedback in V/f control, the motor may lose synchronism during loaded conditions.

I-f open-loop control [5] having a closed-loop current regulation is used to achieve stable operation with full torque capability. After the motor develops sufficient speed with I-f starting, a transition to sensorless vector control is performed. Different transition methods are discussed in the literature to obtain a smooth and seamless changeover. In direct transition methods [6], a quick changeover is performed by changing the control system transformation angle from the synchronously rotating reference frame angle to the already converged sensorless estimated angle. Also, the q-axis current reference and current controller states are redefined appropriately. However, accurate rotor position information is required to achieve a smooth transition. Hence, offset in measurement, the effect of inverter dead-time, and stator resistance variation should be properly compensated. However, a positive d-axis current during I-f control causes motor saturation and results in d-axis inductance variation [7], which is difficult to predict [8, 9]. Furthermore, speed and current oscillations during I-f ramp-up also result in position estimation error with the sensorless algorithm. Consequently, a transition interval is necessary to ensure a smooth variation in stator current and to prevent machine saturation before and after the changeover.

Methods based on increased motor acceleration rate and current profiling are used to reduce motor saturation at the transition instant. A first-order compensator which results in an increased motor acceleration rate is used in [5], such that the synchronously rotating I-f reference frame aligns with the sensorless estimated rotor reference frame. Similarly, a speed-dependent gain is used in [10] for aligning both reference frames. Since the magnitude of the current vector is kept constant in both the methods, the increased motor acceleration rate aligns both reference frames. Thus, variation in stator current and machine saturation is reduced to obtain a smooth transition. However, the successful convergence of these methods depends on compensator parameters.

Current profiling-based methods are also used in the literature to slowly reduce the current vector magnitude so that the synchronously rotating reference frame gets aligned to the sensorless estimated angle. Most of the authors use a linearly decreasing current profile [11–14]. Current profiles, which are inversely proportional to speed [15], exponentially decreasing with time [16], and with a negative slope proportional to the square of error angle [17], are also used. Furthermore, reference current reduction using a closed-loop integral control is proposed in [18]. Even though both increased acceleration rate methods and current profiling methods provide a smooth changeover, a finite time is required for the transition interval. Hence, these methods cannot be used for critical applications such as electric ship propulsion and emergency heat and smoke exhausts, where a quick start-up is necessary.

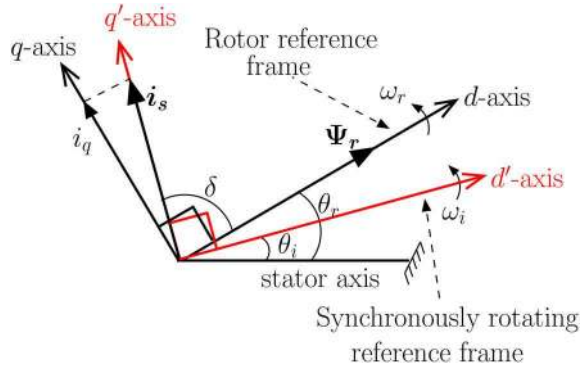

Fig. 1 *Synchronously rotating reference frame and rotor reference frame during I-f open-loop control of PMSM*

A novel pulse-off method is proposed in this paper to achieve a quick and smooth changeover from I-f to sensorless vector control by accurately estimating the rotor angle. In the proposed method, inverter pulses are turned off for a short duration after the motor reaches enough speed for sensorless vector control to work. In the pulse-off duration, the rotor position is estimated using the measured back-emf after the current decreases to zero. Hence, the proposed method accurately determines the rotor position independent of machine parameters such as stator resistance and inductance compared to the conventional direct transition methods. Even though phase/line voltage measurements are commonly used for the control of brushless DC motors [19–22] and for improving the low speed sensorless control of PMSM motors [23–26], this technique is not used for the changeover from I-f control to sensorless control, except in [27]. Since the line voltages are measured during the pulse-off interval, the sensed voltages are devoid of switching frequency components. Hence, no additional filters are required in the proposed method. Also, the complexities and problems involved in high-precision instantaneous voltage measurement methods such as low pass filter (LPF) with compensation [28], analogue integration based [23, 24], voltage controlled oscillator based [25], and digital integrators using fast analogue-to-digital converters [26] are not present. Thus, a simple hall effect based voltage transducers are used in the proposed method. Even though the additional isolated voltage sensors increase cost and number of hardware components, it will not be significant compared to the total system cost in high-power applications, and also of less concern for applications where a quick and reliable starting is the priority. Furthermore, the line voltage sensors can also be used for accurate permanent magnet flux estimation during self-commissioning of PMSM drives.

The proposed method is also used for achieving smooth on-the-fly start during short time power supply interruptions. Since the motor terminal voltages are continuously monitored by a sensorless vector control algorithm, a smooth on-the-fly start is performed without resorting to other complex methods based on signal injection and zero voltage pulse [29–31]. In this paper, in addition to the work presented in [27], a comparison of dynamics of the direct transition method and the proposed method during a changeover is performed using simulation. The transient response of the proposed method is improved by initialising the speed controller with the q-axis current demanded by the load. Also, the time required for current decay during pulse-off is mathematically derived, and used for determining the pulse-off duration for a given drive. Furthermore, the proposed method is experimentally validated on a 25 kW PMSM instead of the low power (2.5 kW) PMSM used in [27].

The paper is organised as follows. In Section 2, I-f open-loop starting, sensorless vector control technique, and the changeover strategies are discussed in detail. Sensorless vector control using a modified stator voltage integration technique is used for medium- and high-speed range control of the drive. Section 3 elaborates on the analysis of the conventional direct transition method. The effect of error in position estimation on the dynamics after the transition is analysed using simulation. The proposed pulse-off method is explained in detail in Section 4. The pulse-off time requirement of the proposed method is mathematically derived in Section 5. The proposed method is experimentally validated in Section 6 and concluded in Section 7.

2 I-f open-loop starting and sensorless vector control

In the I-f method, the motor is accelerated with controlled stator currents. After the motor speed crosses a minimum speed for the sensorless algorithm to operate satisfactorily, a transition to sensorless vector control is performed. I-f control is a speed open-loop and current closed-loop method. In this method, a preset reference speed profile is used as given in (1)

$$\omega_{\mathrm{i}} = K_{\mathrm{w}} t \tag{1}$$

where K_{w} is the slope of speed ramp.

The reference frame transformation angle during I-f control (θ_{i}) is obtained as

$$\theta_{\mathrm{i}} = \int \omega_{\mathrm{i}} \,\mathrm{d}t \tag{2}$$

The stator currents are referred to a synchronously rotating $d' - q'$ reference frame with the transformation angle θ_{i} as shown in Fig. 1. The q'-axis current (i_q') is controlled at the rated value ($I_{q(\mathrm{rated})}$) and the d'-axis current (i_d') is maintained at zero to obtain full torque capability during starting. Thus, the stator current vector ($\boldsymbol{i}_{\mathrm{s}}$) is oriented along the q'-axis. Since the $d' - q'$ reference frame may be shifted from the rotor reference frame (d–q), the machine draws both flux producing d-axis current (i_d) and torque producing q-axis current (i_q) depending on the load.

The I-f starting procedure is divided into the following intervals.

- Kick-off interval
- Ramp-up interval

Kick-off interval: In the kick-off interval, the reference frequency is maintained at a low value to overcome the initial striction and cogging torque. Even though there may be an initial negative speed, the rotor latches to the slowly rotating stator magnetic field. The latching occurs when the load angle reaches a sufficient value such that the generated torque exceeds the total load demand. After the initial kick-off interval, the rotor speed is ramped up according to (1).

Ramp-up interval: The generated torque of a surface-mounted PMSM (SMPMSM) is given by

$$T_{\mathrm{e}} = k_{\mathrm{t}} I_{q(\mathrm{rated})} \sin\delta \tag{3}$$

where k_{t} is the torque constant, $I_{q(\mathrm{rated})}$ is the rated q-axis current and δ is the load angle (angle between the current vector and rotor flux vector). Under stable operation, the generated torque is balanced by the total load demand. Also, for large-signal variation the reference speed (ω_{i}) is assumed to be the same as the rotor speed (ω_{r}). Thus, the generated torque is expressed as

$$k_{\mathrm{t}} I_{q(\mathrm{rated})} \sin\delta = T_{\mathrm{l}} + T_{\mathrm{f}} + B\frac{2}{P}\omega_{\mathrm{i}} + J\frac{2}{P}\frac{\mathrm{d}}{\mathrm{d}t}\omega_{\mathrm{i}} \tag{4}$$

where right-hand side of (4) represents the total load demand, T_{l} is the load torque (Nm), T_{f} is the frictional torque (Nm), J is the moment of inertia (kgm^2), ω_{i} is the electrical reference speed (rad/s), P is the number of poles, and B is the viscous friction coefficient (Nms).

In I-f control, the magnitude of current vector is maintained constant at $I_{q(\mathrm{rated})}$. Hence in (3), only the load angle (δ) is varied to control the generated torque to match the total load demand. The variation of generated torque with load angle (δ) is plotted in Fig. 2.

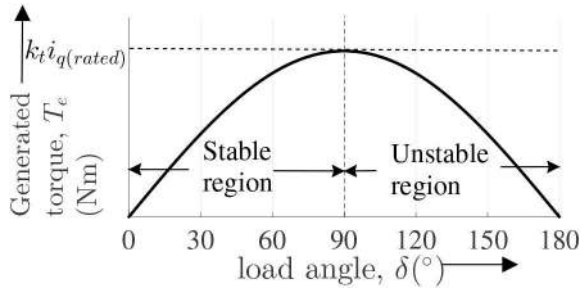

Fig. 2 *Generated torque characteristics of SMPMSM with I-f control*

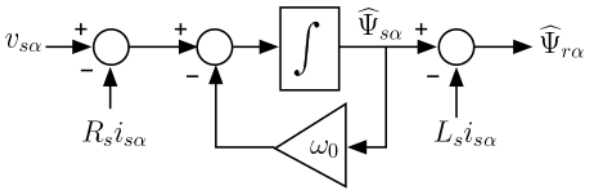

Fig. 3 *Sensorless position estimation using stator voltage integration*

When there is an increased total load demand during speed ramp-up, the acceleration rate of the rotor decreases, resulting in an increase in the load angle. Under stable operation ($0° < \delta < 90°$), when δ increases, the generated torque also increases as seen in Fig. 2. Thus, a new equilibrium point is reached to meet the increased total load demand. Similarly, when the total load demand decreases, the rotor acceleration rate increases and hence δ decreases. From the stable region of Fig. 2 it is observed that the generated torque also decreases when δ decreases, thus maintaining stability. Hence, I-f control has a self-stabilisation action in the region $0° < \delta < 90°$.

However, for $90° < \delta < 180°$ (unstable region in Fig. 2), when the load angle (δ) increases due to the increased total load demand, the generated torque decreases. The decrease in generated torque causes a decrease in rotor acceleration rate, causing a further increase in δ, and finally resulting in loss of synchronism. To ensure stable operation in the ramp-up interval, δ should be limited below 90° even for the worst case total load demand. The worst case total load demand occurs under maximum load torque ($T_{l(max)}$) and maximum viscous friction (assuming a constant T_f). The viscous friction is maximum at the changeover speed (ω_{chg}) during the ramp-up interval. In (4), the slope of reference frequency ($d\omega_r/dt$) is the only control variable that can be chosen to maintain δ below 90°. Thus, loss of synchronism is prevented even under worst case loading condition by fixing the reference frequency slope to a proper value. Let the slope of reference frequency be denoted by a constant 'K_w'. Assuming that the load angle is 90°, the expression for reference frequency slope during ramp-up interval under worst case total load demand is derived from (4) as

$$K_w = K_s \frac{P}{2}\left(\frac{k_t I_{q(rated)} - T_{l(max)} - T_f - B(2/P)\omega_{chg}}{J}\right) \tag{5}$$

where $T_{l(max)}$ is the maximum expected load torque during the ramp-up (Nm) and ω_{chg} is the changeover speed (rad/s). A safety factor K_s is included to incorporate the effect of error in estimated parameters ($K_s < 1$).

Speed and current oscillations occur during the frequency ramp-up interval due to the insufficient damping in the system [32]. These oscillations can even lead to mid-frequency instability, which is an inherent instability of open-loop controlled PMSM without damper windings [33]. In mid-frequency instability, the open-loop control of PMSM becomes unstable beyond a certain operating frequency. The instability may or may not occur depending on the machine parameters, and type of load connected. For machines with large viscous friction or if the connected load is a function of rotor speed, the chance for mid-frequency instability is less due to the high damping in the system. The mid-frequency instability in open-loop I-f controlled PMSM drive is stabilised by modulating the reference speed with the perturbations in input power [34–37], thus adding damping to the overall system. The power perturbation algorithm is included in this paper to improve the damping of speed and current oscillations during open-loop I-f control. When the machine develops enough speed in the ramp-up interval, a changeover to the sensorless vector control is performed.

2.1 Sensorless vector control using modified stator voltage integration

Sensorless vector control methods such as observer-based (Kalman filter, Luenberger observer, or sliding mode observer), high-frequency injection techniques, and estimators using artificial intelligence (neural network and fuzzy-logic based) are used for PMSM drive requiring high-dynamic performance and continuous low-speed control. However, the back-emf-based sensorless technique provides a simple and computationally less intensive solution for applications involving medium- and high-speed range control. In this paper, the sensorless vector control is implemented using a modified stator voltage integration technique [38].

In stator voltage integration, the stator flux vector ($\boldsymbol{\Psi}_s$) is obtained by integrating the stator terminal voltage with resistance drop reduced

$$\boldsymbol{\Psi}_s = \int (\boldsymbol{v}_s - \boldsymbol{i}_s R_s)\, dt \tag{6}$$

where $\boldsymbol{v}_s = v_\alpha + jv_\beta$ is the stator voltage vector, R_s is the stator resistance, and $\boldsymbol{i}_s = i_\alpha + ji_\beta$ is the stator current vector.

The rotor flux vector ($\boldsymbol{\Psi}_r$) is obtained as

$$\boldsymbol{\Psi}_r = \boldsymbol{\Psi}_s - L_s \boldsymbol{i}_s \tag{7}$$

where L_s is the stator inductance.

Sine and cosine of the estimated rotor position ($\hat{\theta}_r$) are given by

$$\cos\hat{\theta}_r = \frac{\hat{\Psi}_{r\alpha}}{|\boldsymbol{\Psi}_r|} \tag{8}$$

$$\sin\hat{\theta}_r = \frac{\hat{\Psi}_{r\beta}}{|\boldsymbol{\Psi}_r|} \tag{9}$$

where $\hat{\Psi}_{r\alpha}$ and $\hat{\Psi}_{r\beta}$ are the α and β components of the estimated rotor flux vector ($\boldsymbol{\Psi}_r$) and $|\boldsymbol{\Psi}_r| = \sqrt{\hat{\Psi}_{r\alpha}^2 + \hat{\Psi}_{r\beta}^2}$.

The rotor speed is estimated from the estimated rotor position as

$$\hat{\omega}_r = \cos\hat{\theta}_r \frac{d}{dt}\left(\sin\hat{\theta}_r\right) - \sin\hat{\theta}_r \frac{d}{dt}\left(\cos\hat{\theta}_r\right) \tag{10}$$

However, the offset in the measured current results in drift in output when a pure integrator is used. To overcome the drift, and to stabilise the integration action, small negative feedback [38] is provided as shown in Fig. 3. Thus, the resulting system acts similar to a LPF. By choosing the corner frequency of LPF (ω_0) as a small value, the transfer function approximates a pure integrator. In the low-speed range, the corner frequency of the LPF is near to the operating speed, causing phase and magnitude error in the estimated rotor flux linkage. Furthermore, inaccuracy in the estimated stator resistance and stator inductance also adds to this error. Hence, to overcome the low-speed issues of the stator voltage integration technique, an open-loop I-f method [32] is used for starting and low-speed operation (0–8 Hz range). The back-emf based sensorless vector control is used only in medium- and high-speed range (above 8 Hz).

2.2 Transition to sensorless vector control

Increased acceleration rate and current profiling-based methods are used to achieve a smooth changeover from I-f control to sensorless vector control. However, for critical applications requiring a quick

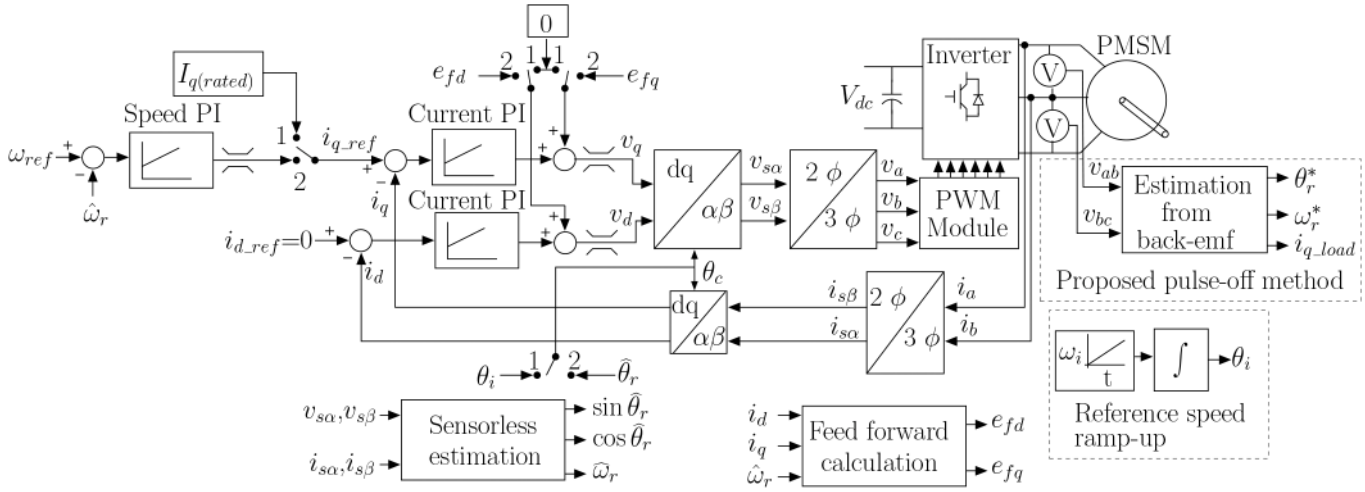

Fig. 4 *Control system for sensorless vector control of PMSM with I-f starting*

Table 1 PMSM parameters

rated power	25 kW	permanent-magnet flux	0.185 Wb
rated speed	3000 rpm	*d*-axis inductance	0.168 mH
rated frequency	400 Hz	*q*-axis inductance	0.178 mH
rated torque	80 Nm	stator resistance	29 mΩ
root-mean-square line voltage	400 V	inertia	2 kgm^2
rated current	35 A	Pole pairs	8

start-up, a direct transition method devoid of a transition interval is conventionally used. The changeover is performed at about 5–10% of rated speed based on the assumption that the estimated position has already converged. To achieve a smooth transition, the transformation angle and *q*-axis current reference should be properly initialised. However, the convergence of the estimated position highly depends on the system parameters. Furthermore, speed oscillations during the I-f ramp-up due to mid-frequency instability also cause estimation error in the direct transition method. Hence, the direct transition is performed at a constant speed, where the speed oscillations have already settled [6]. A detailed analysis of the effect of error in position estimation at the changeover instant on the system dynamics after the changeover is analysed in Section 3 using simulation.

The proposed pulse-off method estimates the position from measured back-emf and does not depend on the sensorless estimated position at the transition. Hence, a constant speed interval for speed oscillations to settle is not required for the proposed method. A changeover to sensorless vector control is performed during the I-f ramp-up interval, achieving a quick start-up as demonstrated in the experimental results in Section 6. The proposed method is discussed in detail in Section 4.

3 Analysis of direct transition method

The direct transition method is implemented in the system shown in Fig. 4 (devoid of the proposed method block) and simulated in MATLAB/Simulink. A 25 kW PMSM with parameters given in Table 1 is used for the study. The simulation results while using the direct transition method are shown in Fig. 5. A constant load torque of 25 Nm is considered for all simulations. The machine is started with a kick-off interval of 2 s with the machine speed maintained at 1 Hz. After the kick-off interval, the machine speed is ramped up at a rate of 5 Hz/s to reach a steady-state speed of 10 Hz. In spite of the power perturbation algorithm, damped oscillations are observed in the speed and current waveforms during both kick-off and ramp-up interval. The magnitude of oscillations would have been larger with a longer settling time if the I-f control was performed without power perturbation stabilisation. A transition to sensorless vector control is performed at 5 s, once the oscillations are settled. The transition is performed by changing all the switch positions in

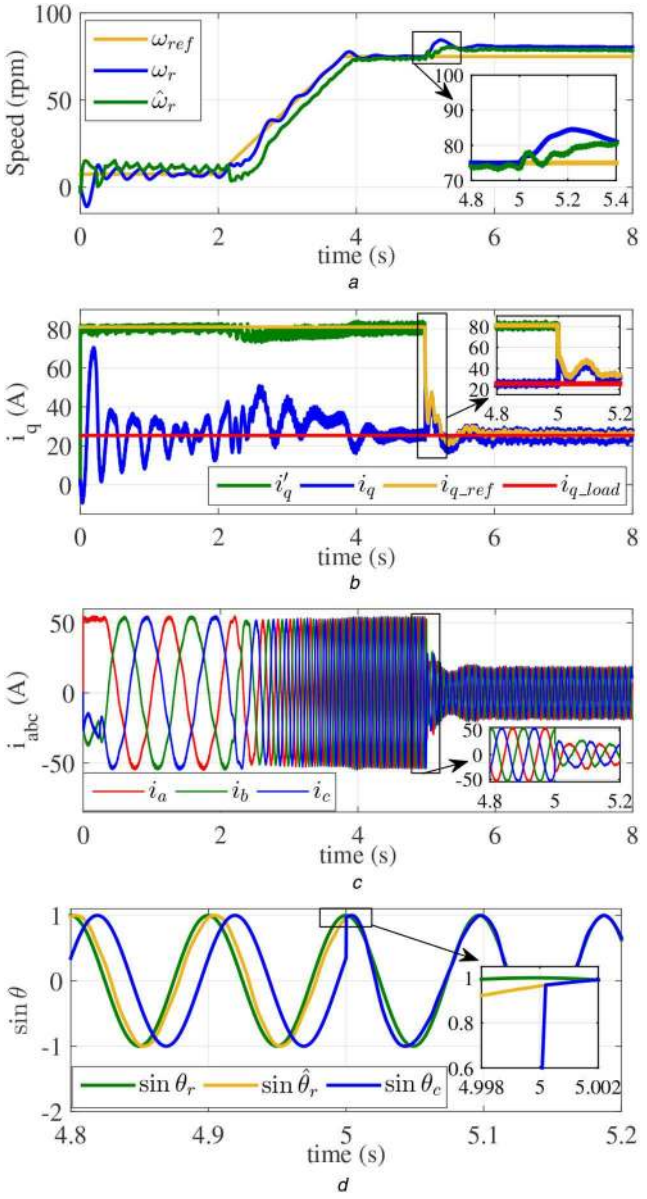

Fig. 5 *Simulation results of direct transition method at the changeover*
(a) Speed waveforms, ***(b)*** *q*-axis current waveforms, ***(c)*** Phase current waveform, ***(d)*** sin *θ* waveforms

Fig. 4 from 1 to 2. The reference frame transformation angle (θ_c), which is derived from θ_i during I-f control is changed to $\hat{\theta}_r$ in

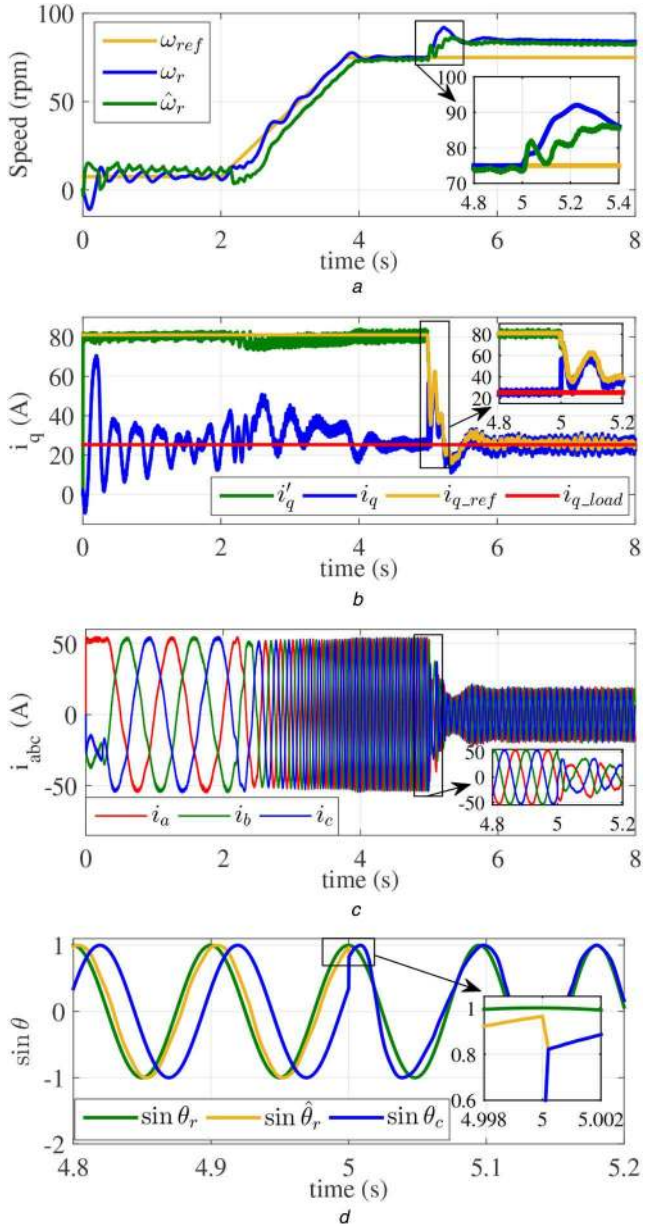

Fig. 6 *Simulation results of direct transition with 15% additional error at the changeover*

(a) Speed waveforms, ***(b)*** q-axis current waveforms, ***(c)*** Phase current waveform, ***(d)*** sin θ waveforms

sensorless vector control as shown in Fig. 5*d*. 'i_{q_load}' in Fig. 5*b* represents the q-axis current demanded by the load. i_{q_load} is 25.3 A for the considered machine with 25 Nm load. q'-axis current is maintained at a constant reference during I-f control, thereby maintaining the stator currents at a rated value as observed from Figs. 5*b* and *c*. The actual q-axis current (i_q) oscillates about i_{q_load} in the kick-off interval and has a mean value above i_{q_load} for acceleration in the ramp-up interval. Since the actual q-axis current (i_q) is proportional to the generated torque for SMPMSM, i_q represents the generated torque itself.

Even though the sensorless algorithm uses accurate machine parameters, oscillations in speed and current are observed after the transition to sensorless vector control. The oscillations arise due to the error in the estimated rotor position at the transition instant as observed in Fig. 5*d*. The control system transformation angle (θ_c) is initialised to the sensorless estimated rotor position ($\hat{\theta}_r$) instead of the actual rotor angle (θ_r). The small error in estimated position is due to the use of LPF instead of a pure integrator for stator voltage integration. The magnitude of error is proportional to the proximity of operating frequency to the corner frequency of LPF (1 Hz). The error in estimated rotor position causes an error in the estimated speed and initial value of q-axis current reference (i_{q_ref}) for sensorless vector control initialisation after the transition instant. The q-axis current reference should ideally reset to i_{q_load} (25.3 A) to achieve a smooth transition but instead reset to 50.8 A as shown in the inset of Fig. 5*b*. Furthermore, error in estimated speed also adds to additional oscillations in i_{q_ref} due to the proportional action of the speed controller after the changeover.

Variation in motor parameters such as stator resistance due to temperature and saturation of d-axis inductance causes additional magnitude and phase error in the estimated rotor flux in sensorless vector control. Furthermore, the effect of dead-band, cogging torque at low speed and inaccurate inverter modelling cause low-frequency oscillations (fifth and seventh harmonic) in the estimated rotor flux. Compensation techniques are normally used to compensate for stator resistance variation, the effect of dead-time and modelling errors of the inverter. However, the resulting sensorless algorithm becomes highly complex while using such techniques. Also, the effects of d-axis inductance saturation and cross-coupling magnetisation are difficult to predict as explained before. Low-frequency oscillations during I-f starting also result in inaccuracies in the estimated rotor position. In this paper, the modified stator voltage integration-based sensorless algorithm is used without additional compensation techniques for implementing both the direct transition method and the proposed pulse-off method. To incorporate the effect of parameter variation, inverter dead-time, cogging torque, inaccurate inverter modelling, and error due to speed oscillations, an error of 15% is added to the sine of the sensorless estimated position at the transition instant. Let $\sin\theta_{err}$ be the sine of estimated sensorless position with 15% error. The resulting erroneous cosine of estimated angle is computed as $\sqrt{1-\sin\theta_{err}}$. Fig. 6 shows the simulation result of the direct transition method with an additional error of 15% added to the estimated position at the transition instant. A larger magnitude of speed and current oscillations is observed after transition compared to the direct transition method without additional error. The i_{q_ref} is initialised to 71.7 A instead for 25.3 A demanded by the load torque as seen from the inset of Fig. 6*b*. The higher value of initial i_{q_ref} increases the generated torque momentarily accelerating the machine to a higher speed even though the machine is already at the reference speed. Consequently, the machine takes a longer time to settle to the reference speed due to the slow action of integral control in the speed proportional–integral (PI) controller as observed in Fig. 6*a*.

4 Proposed pulse-off method

In the proposed pulse-off method, the rotor position at changeover is obtained from line voltage measurement instead of relying on sensorless vector control. Thus, an accurate rotor position is obtained independent of machine parameters and speed oscillations at low speed to achieve a quick and smooth transition. In this method, when the motor speed reaches the changeover speed, the inverter pulses are disabled for a short duration. Therefore, the stator currents decrease to zero through the freewheeling diodes. The machine internal back-emf is reflected in the measured line voltage when the current reduces to zero.

Assuming a sinusoidal back-emf, the back-emf vector ($\boldsymbol{e}_b$) and rotor flux vector are related by

$$\boldsymbol{e}_b = \frac{d\boldsymbol{\Psi}_r}{dt} \tag{11}$$

Furthermore, the rotor position of PMSM is the same as the rotor flux position. Thus, the rotor position is estimated in the pulse-off interval from the measured line voltages.

The assumption of sinusoidal back-emf is applicable only if the harmonics in back-emf are not significant. Hence, the proposed method is only applicable to sinusoidal back-emf machines with less amount of other harmonics. Methods such as skewing and fractional slot windings [39] are conventionally used to reduce the higher-order harmonics (due to slot harmonics) in the back-emf.

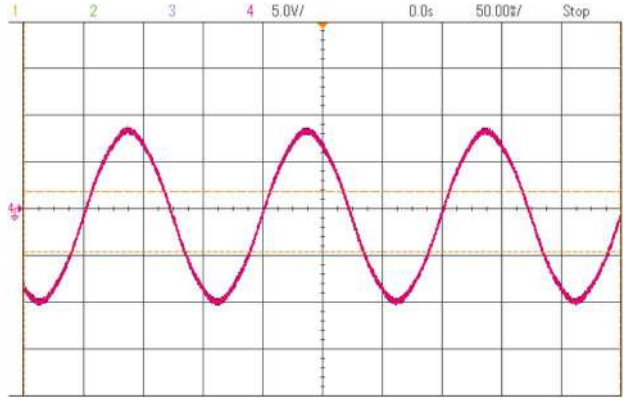

Fig. 7 *Measured line-line back-emf voltage of the 25 kW PMSM: Ch4 – v_{ab} (X-axis: 50 ms/div; Y-axis: 5 V/div)*

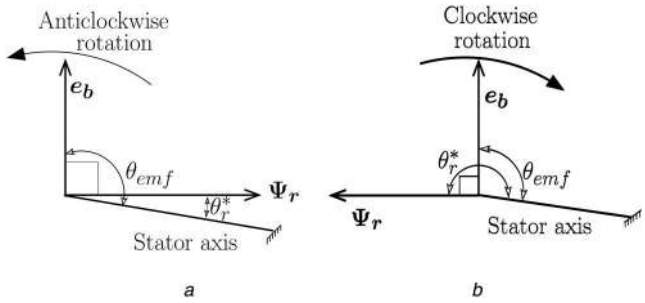

Fig. 8 *Relative position of back-emf and rotor flux vectors*
(a) Case 1, ***(b)*** Case 2

The back-emf of 25 kW PMSM with fractional slot winding used in this paper is shown in Fig. 7.

The back-emf vector ($\boldsymbol{e}_b = e_\alpha + je_\beta$) is computed from the two measured line voltages as

$$e_\alpha = v_{ab} + \frac{v_{bc}}{2} \tag{12}$$

$$e_\beta = \frac{\sqrt{3}}{2} v_{bc} \tag{13}$$

Sine and cosine of back-emf vector position are given by

$$\cos(\theta_{\text{emf}}) = \frac{e_\alpha}{|\boldsymbol{e}|} \tag{14}$$

$$\sin(\theta_{\text{emf}}) = \frac{e_\beta}{|\boldsymbol{e}|} \tag{15}$$

where θ_{emf} is the position of the back-emf vector with respect to the stationary a-phase axis, and $|\boldsymbol{e}| = \sqrt{e_\alpha^2 + e_\beta^2}$ is the magnitude of back-emf vector. Let θ_{r}^* denote the estimated rotor position using the pulse-off method. The rotor flux vector lags back-emf by 90°. Hence, during anticlockwise rotation $\theta_{\text{r}}^* = \theta_{\text{emf}} - 90°$ as is observed in Fig. 8*a*. However, during clockwise rotation, $\theta_{\text{r}}^* = \theta_{\text{emf}} + 90°$ as observed in Fig. 8*b*.

Sine and cosine of rotor flux position during anticlockwise rotation are expressed as

$$\sin(\theta_{\text{r}}^*) = \sin(\theta_{\text{emf}} - 90°) = -\cos\theta_{\text{emf}} \tag{16}$$

$$\cos(\theta_{\text{r}}^*) = \cos(\theta_{\text{emf}} - 90°) = \sin\theta_{\text{emf}} \tag{17}$$

Sine and cosine of rotor flux position during clockwise rotation is obtained as

$$\sin(\theta_{\text{r}}^*) = \sin(\theta_{\text{emf}} + 90°) = \cos\theta_{\text{emf}} \tag{18}$$

$$\cos(\theta_{\text{r}}^*) = \cos(\theta_{\text{emf}} + 90°) = -\sin\theta_{\text{emf}} \tag{19}$$

The estimated rotor speed using the pulse-off method (ω_{r}^*) is given by

$$\omega_{\text{r}}^* = \cos\theta_{\text{r}}^* \frac{\text{d}}{\text{d}t}(\sin\theta_{\text{r}}^*) - \sin\theta_{\text{r}}^* \frac{\text{d}}{\text{d}t}(\cos\theta_{\text{r}}^*) \tag{20}$$

An accurate estimate of permanent magnet flux linkage (Ψ_{F}) is necessary for the control system to compute the feed forward of machine back-emf. However, due to demagnetisation and ageing, Ψ_{F} reduces from its original value. In the proposed method, Ψ_{F} is estimated in the pulse-off duration using the measured back-emf and estimated speed. The estimated permanent magnet flux linkage using the pulse-off method (Ψ_{F}^*) is obtained as

$$\Psi_{\text{F}}^* = \frac{|\boldsymbol{e}_{\text{b}}|}{\omega_{\text{r}}^*} \tag{21}$$

Thus, Ψ_{F} in the feed forward calculation is updated in every drive start-up during the pulse-off interval.

The control is transferred from the I-f method to sensorless vector control by enabling the inverter pulses, once the rotor position, rotor speed, and q-axis current demand of load are computed. The estimated rotor position is used to initialise the integrator in the sensorless module. Furthermore, the estimated speed during pulse-off is used to initialise the speed filter. However, to achieve a smooth transition, the speed controller also should be initialised appropriately with the q-axis current demanded by load torque at the transition. A wrong initialisation of integral control produces a higher or lower generated torque resulting in unwanted oscillations in speed and current as discussed in Section 3. The computation of q-axis current demand by the load for speed PI controller initialisation is discussed as follows.

4.1 Computation of q-axis current demanded by the load

The generated torque of PMSM supplies the total load torque ($T_{\text{l}} + T_{\text{f}} + B(2/P)\omega_{\text{r}}$) and is used for acceleration as observed in (4). Hence, the q-axis current demanded by the load (i_{q_load}) before pulse-off is obtained as

$$i_{q\_\text{load}} = \frac{T_{\text{e}} - J(2/P)(\text{d}/\text{d}t)\omega_{\text{r}}}{k_{\text{t}}} \tag{22}$$

$$= I_{q(\text{rated})}\sin\delta - \frac{J}{k_{\text{t}}}\frac{2}{P}\frac{\text{d}}{\text{d}t}\omega_{\text{r}} \tag{23}$$

From Fig. 1, the load angle is obtained as

$$\delta = 90° + \theta_{\text{i}} - \theta_{\text{r}}^* \tag{24}$$

where θ_{i} is the synchronously rotating reference frame angle in I-f control and θ_{r}^* is the rotor angle estimated from back-emf.

However, θ_{i} and θ_{r}^* cannot be computed at the same time instant. θ_{i} is used to control the current vector only till the starting instant of pulse-off, whereas θ_{r}^* is computed only by the end of pulse-off duration. Hence, θ_{r}^* at the end of the pulse-off interval (θ_{r1}^*) is interpolated to the start of pulse-off duration (θ_{r0}^*) to estimate the q-axis current demanded by the load. The rotor speed is assumed as constant during the pulse-off duration due to the large inertia of the considered machine. θ_{r}^* at the beginning of pulse-off interval (θ_{r0}^*) is given by

$$\theta_{\text{r0}}^* = \theta_{\text{r1}}^* - \omega_{\text{r}}^* t_{\text{off}} \tag{25}$$

where t_{off} is the pulse-off duration.

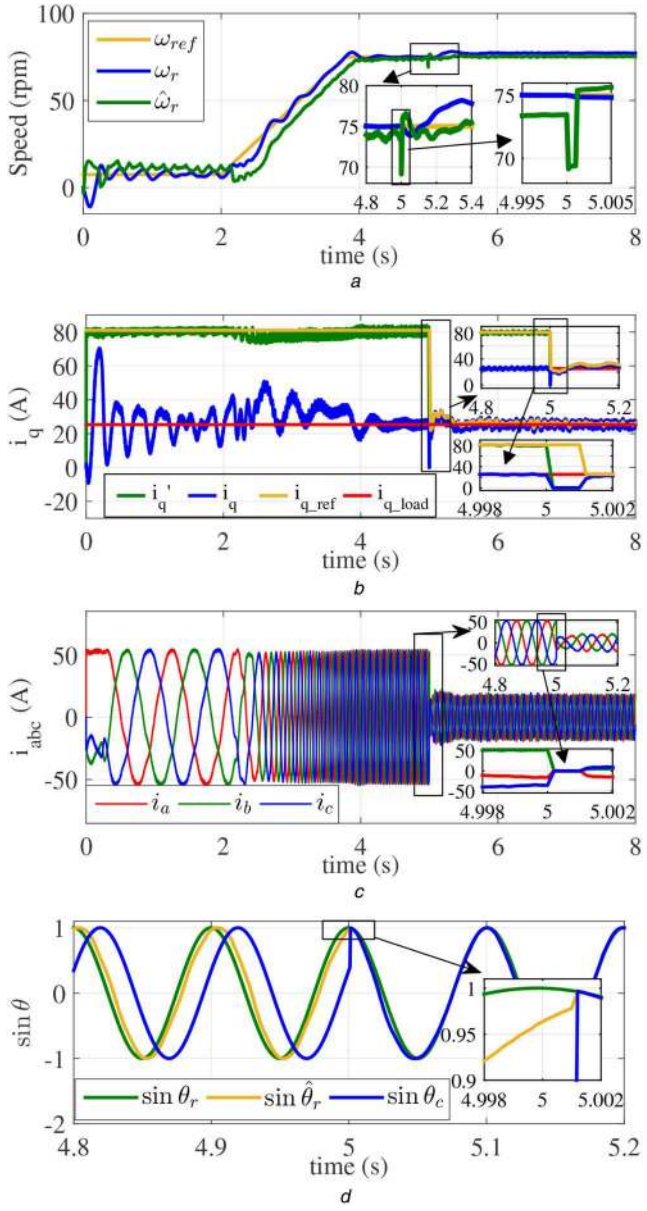

Fig. 9 *Simulation results of the proposed pulse-off method*
(a) Speed waveforms, ***(b)*** q-axis current waveforms, ***(c)*** Phase current waveform, ***(d)*** sin θ waveforms

Table 2 Performance comparison of various transition methods

	Magnitude of maximum overshoot after the transition		
	In motor speed (ω_r), rpm	In q-axis current (i_q), A	In a-phase current (i_a), A
direct transition method	9.5	21.7	14.5
direct transition method with 15% additional error	17	34.7	23.1
proposed pulse-off method	3.2	8.3	5.5

The q-axis current demanded by the load torque for speed controller initialisation when the changeover is performed in ramp-up interval is obtained as

$$i_{q\_\text{init}} = I_{q(\text{rated})}\cos(\theta_{i0} - \theta^*_{r0}) - \frac{J}{k_t}\frac{2}{P}K_w \tag{26}$$

where θ_{i0} is the synchronous reference frame transformation angle at the instant before pulse-off and K_w is the slope of speed ramp in I-f control.

However, the acceleration torque is not present when the changeover is performed in the constant speed interval after the speed ramp-up. Hence, the q-axis current demanded by the load torque in the constant speed interval is given by

$$i_{q\_\text{init}} = I_{q(\text{rated})}\cos(\theta_{i0} - \theta^*_{r0}) \tag{27}$$

4.2 Simulation of the proposed method

The control block diagram of the proposed method is shown in Fig. 4. The proposed method is implemented on a 25 kW PMSM drive with the parameters in Table 1 and simulated in MATLAB/Simulink to evaluate its performance. Similar to the direct transition method, I-f control is used to ramp-up the speed initially. However, instead of directly changing all the switch positions from 1 to 2 in Fig. 4, a pulse-off interval of 1 ms is provided at the transition instant. The rotor position, rotor speed, and q-axis current demanded by the load are estimated, and the corresponding integrators are initialised as discussed before. A smooth transition is observed in the speed waveform in Fig. 9*a* and the current waveforms in Figs. 9*b* and *c*. The rotor position is estimated accurately from the sensed line voltages, and the sensorless position is corrected at the end of the pulse-off interval as seen in Fig. 9*d*. From the inset of Fig. 9*b*, it is observed that the reference q-axis current is also initialised to i_{q_load} in the proposed method. As a result, the oscillations in speed and phase currents are minimised. The small oscillations are due to the inaccuracies in sensorless vector control after the changeover. However, the oscillations are reduced significantly compared to both the direct transition method and the direct transition method with an additional error. A comparison of the performance of the proposed pulse-off method with the direct transition method and direct transition method with 15% additional error is shown in Table 2 for better clarity.

4.3 On-the-fly starting for power failure ride through

The proposed method is also extended to achieve on-the-fly start of PMSM. During short-time power failure, the inverter pulses are disabled to prevent the DC bus discharge and consequent under voltage trip. When the supply is restored after a short time power failure, the motor will be in motion due to the stored kinetic energy. In industries, to prevent the monetary loss that would occur due to a complete system restart after waiting for the motor to reach zero speed, the motor is started on-the-fly with sensorless vector control. The line voltage sensors in the proposed method are used to estimate the rotor position continuously during the supply failure interval. Similar to the pulse-off method, the motor is started directly in sensorless vector control when the supply is restored by properly initialising the speed controller, speed filter, and the integrator in the sensorless module. However, for directly starting with sensorless vector control, the motor speed should not fall below the changeover speed of the pulse-off method. The motor deceleration during supply failure depends on the motor inertia and the load torque.

5 Determination of the pulse-off time

A finite time is required for the stator currents to decay to zero depending on DC bus voltage, instantaneous motor currents, and stator inductance during pulse-off. Also, accurate position estimation is obtained with the proposed method when the back-emf is estimated at zero current. Hence, the duration of pulse-off should be selected such that all currents become zero even in the worst case before re-enabling the pulses. In this section, the worst-case time required for current decay is analytically derived. The pulse-off time is fixed by providing an extra margin to the worst-case current decay time.

The stator current directions are assumed as given in Fig. 10 at the pulse-off instant. When the pulses are disabled, the highlighted

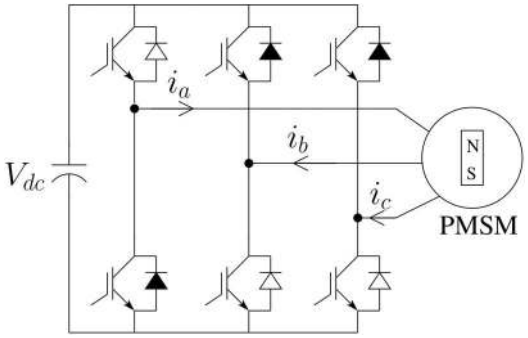

Fig. 10 *PMSM supplied from the inverter*

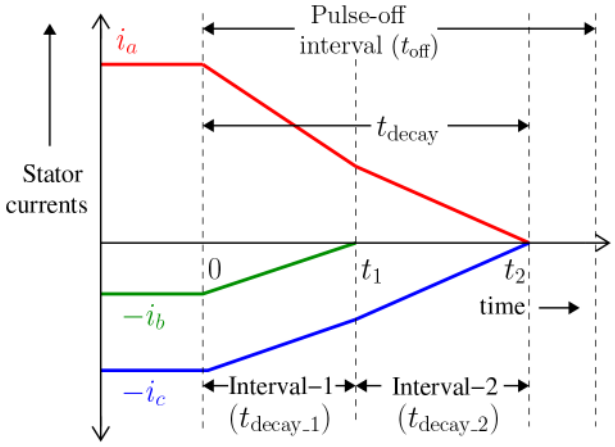

Fig. 11 *Stator current decay during the pulse-off interval*

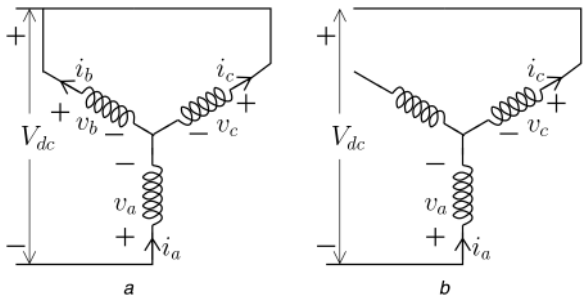

Fig. 12 *Equivalent circuit of PMSM under pulse-off interval*
(a) Interval 1, ***(b)*** Interval 2

diodes in Fig. 10 conducts and the stator currents decay to zero as presented in Fig. 11. The resulting equivalent circuit is shown in Fig. 12*a*. This initial time interval with three non-zero currents is termed as interval-1. However, the smallest current first decays to zero resulting in an equivalent circuit shown in Fig. 12*b*. Interval-2 denotes the time interval with only two non-zero currents. Depending on the instantaneous currents at the pulse-off instant, either interval-1 alone, or interval-2 alone or both interval 1 and 2 may be present. The time duration for interval-1 and interval-2 are analytically derived in the following section.

5.1 Calculation of interval-1 time duration

During the stator current decay in pulse-off duration, the full DC bus voltage gets applied across the stator terminals. Since the motor speed is very low at the transition interval, the back-emf voltage of PMSM is small compared to the DC bus voltage (V_{dc}). Hence, to simplify the calculation of stator current decay time, the stator resistance and the back-emf are neglected in the stator voltage equation of PMSM. The resulting equation is given by

$$v_a = (L_{ls} + L_{ms})\frac{di_a}{dt} + 0.5L_{ms}\frac{di_b}{dt} + 0.5L_{ms}\frac{di_c}{dt} \tag{28}$$

$$v_b = -0.5L_{ms}\frac{di_a}{dt} - (L_{ls} + L_{ms})\frac{di_b}{dt} + 0.5L_{ms}\frac{di_c}{dt} \tag{29}$$

$$v_c = -0.5L_{ms}\frac{di_a}{dt} + 0.5L_{ms}\frac{di_b}{dt} - (L_{ls} + L_{ms})\frac{di_c}{dt} \tag{30}$$

where L_{ls} is the leakage inductance and L_{ms} is the magnetising inductance.

From the equivalent circuit in Fig. 12*a*, it is observed that $v_b = v_c$ and $i_a = i_b + i_c$. Hence, the relation between derivatives of stator currents is obtained by equating (29) and (30) and using $(di_a/dt) = (di_b/dt) + (di_c/dt)$ as

$$\frac{di_a}{dt} = 2\frac{di_b}{dt} = 2\frac{di_c}{dt} \tag{31}$$

The DC bus voltage equation is derived by using (31), (28) and (29) as

$$V_{dc} = v_b - v_a = -1.5\left(L_{ls} + \frac{3}{2}L_{ms}\right)\frac{di_a}{dt} \tag{32}$$

$$= -1.5L_0\frac{di_a}{dt} \tag{33}$$

where $L_0 = L_{ls} + (3/2)L_{ms}$.

Let i_b be the smallest current at the pulse-off instant. The slope of the smallest current at the pulse-off instant in interval-1 (m_{1_small}) is obtained by using (33) and (31) as

$$m_{1\_small} = \frac{di_b}{dt} = -\frac{V_{dc}}{3L_0} \tag{34}$$

Hence, the time duration of interval-1 (t_{decay_1}) is given by

$$t_{decay\_1} = \frac{-i_{small}(0)}{m_{1\_small}} = \frac{-i_b(0)}{m_{1\_small}} \tag{35}$$

$$= \frac{3L_0 i_b(0)}{V_{dc}} \tag{36}$$

where $i_{small}(0)$ is the magnitude of i_{small} (the smallest current at the instant of pulse-off) at the instant '0' and $i_b(0)$ is the *b*-phase current at the instant of pulse-off.

5.2 Calculation of interval-2 time duration

When the smallest current at pulse-off instant decays to zero, the equivalent circuit changes to Fig. 12*b*, initiating interval-2 operation. From Fig. 12*b*, it is observed that in interval-2, $i_a = i_c$ and hence $di_a/dt = di_c/dt$.

The DC bus voltage expression is obtained using (28) and (30) as

$$V_{dc} = v_c - v_a \tag{37}$$

$$= -2L_0\frac{di_a}{dt} \tag{38}$$

The slope of the largest current at a pulse-off instant (i_a in this case) during interval-2 (m_{2_large}) is obtained from (38) as

$$m_{2\_large} = \frac{di_a}{dt} = -\frac{V_{dc}}{2L_0} \tag{39}$$

Thus, the time duration of interval-2 (t_{decay_2}) is given by

$$t_{decay\_2} = \frac{-i_{large}(t_1)}{m_{2\_large}} = \frac{-i_a(t_1)}{m_{2\_large}} \tag{40}$$

$$= \frac{2L_0 i_a(t_1)}{V_{dc}} \quad (41)$$

where $i_a(t_1) = i_a(0) + 2m_{1\_small}\, t_{decay\_1}$, '$i_a(t_1)$' is the magnitude of a-phase current at the instant t_1, '$i_{large}(t_1)$' is the magnitude of i_{large} (largest current at a pulse-off instant) at instant t_1.

5.3 Calculation of total stator current decay time

Finally, the total time duration of stator current decay is obtained using (36) and (41) as

$$t_{decay} = t_{decay\_1} + t_{decay\_2} \quad (42)$$

$$= \frac{L_0}{V_{dc}}\left(2\, i_{large}(0) - i_{small}(0)\right) \quad (43)$$

$$= \frac{L_0}{V_{dc}}\left(2\, i_a(0) - i_b(0)\right) \quad (44)$$

For interior PMSM, L_0 varies between d-axis inductance (L_d) and q-axis inductance (L_q) depending on the rotor position. Furthermore, $i_{large}(0)$ and $i_{small}(0)$ are the magnitude of instantaneous currents at the pulse-off instant.

Variation of instantaneous stator currents with the current vector angle (ϵ) is shown in Fig. 13. The a-phase, b-phase or c-phase cyclically becomes the largest or the smallest phase current in every 30° interval. Hence, the limiting case of t_{decay} is captured when ϵ is varied from 0° to 30°. When $\epsilon = 30°$, the smallest current at pulse-off instant $i_{small}(0) = 0$. This corresponds to the condition where only interval-2 is present ($t_{decay\_1} = 0$). When $\epsilon = 0°$, the largest current becomes zero by the end of interval-1 ($i_{large}(t_1) = 0$). This represents the condition where only interval-1 is present ($t_{decay\_2} = 0$). The plot of current decay time obtained using (44) for ϵ variation in the range $0° - 30°$ with both $L_0 = L_d$ and $L_0 = L_q$ is shown in Fig. 14. The stator current decay time for a particular operation could be anywhere between the two limits. However, the pulse-off duration should be designed considering the worst case of decay time. The maximum current decay time (38.57 μs) occurs at $\epsilon = 30°$ with the current vector aligned along the rotor q-axis ($L_0 = L_q$). Finally, the pulse-off time is fixed as 500 μs for the experiments considering a safety margin and the additional time for the computations. Since the moment of inertia is large enough, the pulse-off time will not cause a significant speed reduction. The speed reduction occurred during the pulse-off interval is calculated in Section 6.

6 Experimental validation

The proposed pulse-off method is validated on a 25 kW PMSM drive whose parameters are given in Table 1. The PMSM is coupled to a DC generator for loading as shown in Fig. 15. TMS320F28335 digital signal processor is used as the control platform and the inverter switching frequency is selected as 5 kHz. A kick-off interval of 0.5 s with a constant frequency of 2 Hz is provided. After the kick-off interval, the machine is ramped up at 20 Hz/s and a changeover is performed at 8 Hz. A pulse-off duration of 500 μs is provided when the reference speed reaches 8 Hz. The a-phase current and speed waveform under loaded and no-load condition are shown in Figs. 16 and 17, respectively. In both loaded and unloaded cases, rated current is drawn by the machine during I-f start-up since the current vector magnitude is held constant by the control. Even after the transition, the machine draws full rated current to quickly ramp-up to the reference speed with full rated torque. However, during sensorless vector control, only the q-axis current proportional to load torque is drawn by the machine, and the d-axis current is controlled at zero. Hence, at the steady-state operation of sensorless vector control, a higher current is drawn by the machine in the loaded case compared to the unloaded case as observed in Figs. 16 and 17. A smooth changeover is observed in current with the proposed method. Even

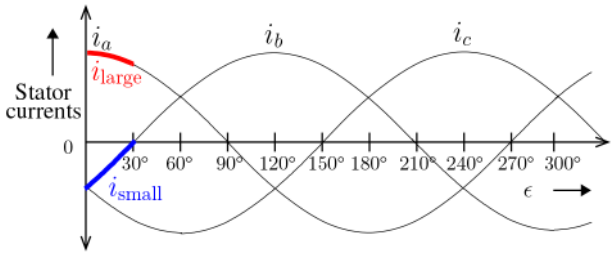

Fig. 13 *Variation of stator currents with current vector angle*

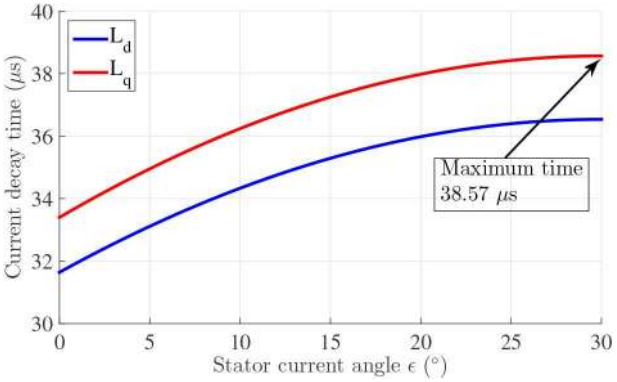

Fig. 14 *Stator current decay time variation during pulse-off*

Fig. 15 *Experimental setup of 25 kW PMSM drive*

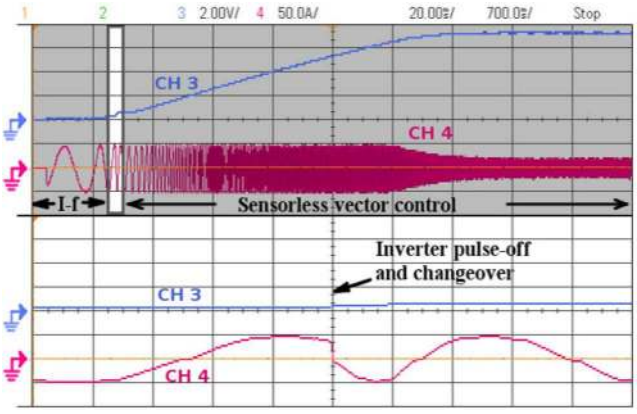

Fig. 16 *Speed and stator current waveforms with pulse-off method under loaded condition. Ch3: $\hat{\omega}_r$, Ch4: i_a (X-axis: 0.7 s/div; Y-axis: Ch3: 240 mech. rpm/div, Ch4: 50 A/div)*

though the generated torque falls to zero for a short duration in the pulse-off interval, dip in speed is not observed in both loaded and no-load conditions. The moderately high inertia of the machine (2 kg m^2) is sufficient to maintain the machine speed in the pulse-off duration.

Since the stator currents decay to zero in the pulse-off interval, the generated torque also becomes zero. Hence, a reduction in speed occurs depending on the load present and the machine inertia. Since the reduction in speed is reflected in the back-emf vector position, the proposed method remains unaffected by the

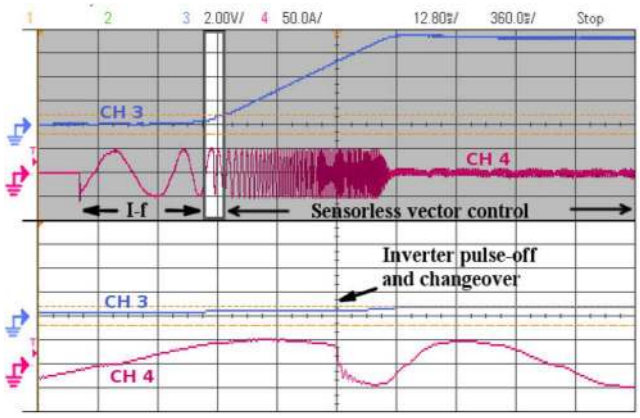

Fig. 17 *Speed and stator current waveforms with pulse-off method under no-load. Ch3: $\hat{\omega}_r$, Ch4: i_a (X-axis: 0.36 s/div; Y-axis: Ch3: 240 mech. rpm/div, Ch4: 50 A/div)*

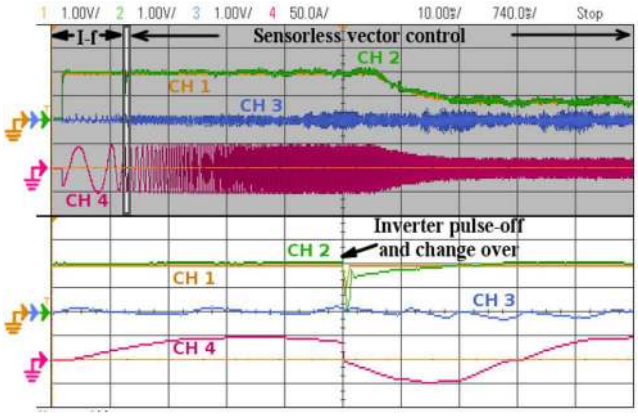

Fig. 18 *Variation of d-axis and q-axis currents with pulse-off method under loaded condition. Ch1: i_{q_ref}, Ch2: i'_q, Ch3: i'_d, Ch4: i_a (X-axis: 0.74 s/div; Y-axis: Ch1, Ch2 ,Ch3: 40 A/div, Ch4: 50 A/div)*

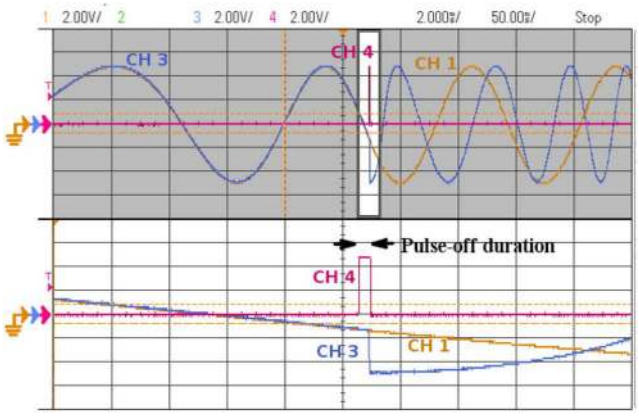

Fig. 19 *Variation of control system transformation angle with the pulse-off method at the transition instant. Ch1: θ_i, Ch3: θ_c, Ch4: pulse-off signal (X-axis: 50 ms/div; Y-axis: Ch1, Ch3, Ch4: 0.4 unit/div)*

speed dip. However, while using the proposed method for a given system, the speed should not fall below the minimum speed for sensorless algorithm operation during the pulse-off interval. Hence, the worst-case dip in speed during the pulse-off interval under full load should be assessed for every system, and the changeover speed should be selected accordingly. For the 25 kW PMSM, the worst-case speed dip is obtained as

$$\Delta\omega = \frac{T_{l(\max)}\, t_{\text{off}}}{J} = \frac{80 \times \left(500 \times 10^{-6}\right)}{2} \tag{45}$$

$$= 0.02\,\text{rad/s} \tag{46}$$

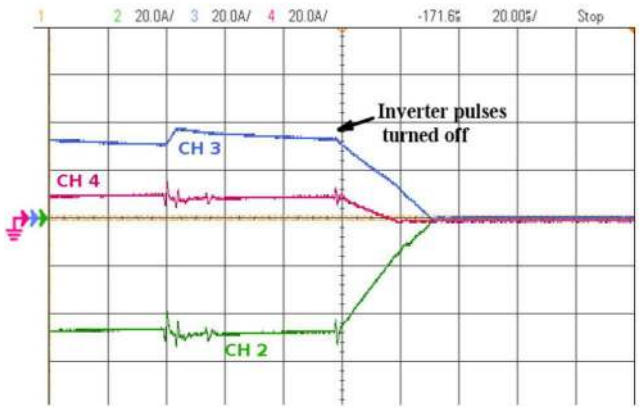

Fig. 20 *Stator current waveforms in the pulse-off duration. Ch2: i_a, Ch3: i_b, Ch4: i_c (X-axis: 20 μs/div; Y-axis: Ch2,Ch3,Ch4: 20 A/div*

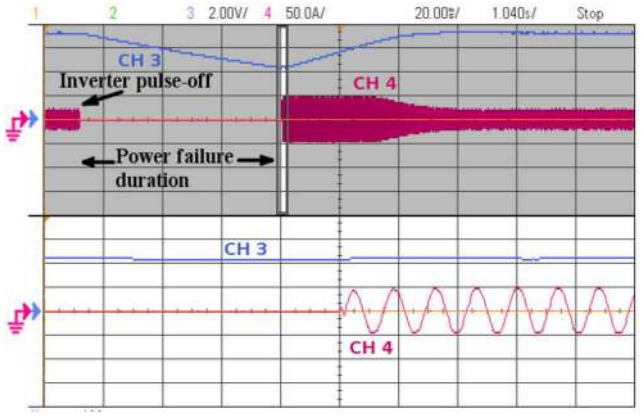

Fig. 21 *Speed and stator current waveforms during on-the-fly start with pulse-off method under loaded condition. Ch3: $\hat{\omega}_r$, Ch4: i_a (X-axis: 1.04 s/div; Y-axis: Ch3: 240 mech. rpm/div, Ch4: 50 A/div)*

Thus, a negligible speed dip occurs as verified by the experimental results.

d- and *q*-axis current waveforms under loaded conditions are shown in Fig. 18. After the pulse-off duration, the integrator in the speed controller is initialised with an accurate value of *q*-axis current demanded by the load. Thus, the transients in *q*-axis current reference quickly settle after the transition. The control system transformation angle (θ_c) is equal to synchronously rotating reference frame angle (θ_i) till the transition instant as observed in Fig. 19. During the pulse-off interval, the rotor position is estimated from back-emf, and the integrator in the sensorless algorithm is initialised appropriately. After the transition to sensorless vector control, the control system transformation angle (θ_c) denotes the sensorless vector control angle ($\hat{\theta}_r$) itself.

The three-phase current waveforms in the pulse-off interval are shown in Fig. 20. Nearly 33 μs is required for the stator currents to decay, which is within the calculated range given in Fig. 14. Also, the two intervals of the pulse-off process are clearly visible in Fig. 20. *a*-phase current and speed waveforms during on-the-fly starting of PMSM under loaded and no-load conditions are shown in Figs. 21 and 22. As soon as the supply is restored, the machine is started directly with sensorless vector control. The currents are quickly increased to the rated value without any oscillations. The quick current control action is achieved by accurate position estimation using the proposed method.

Figs. 23 and 24 show *d*- and *q*-axis current waveforms during on-the-fly starting, under loaded and no-load condition, respectively. The *q*-axis current is quickly regulated at the rated value and *d*-axis current is maintained at zero after the transition.

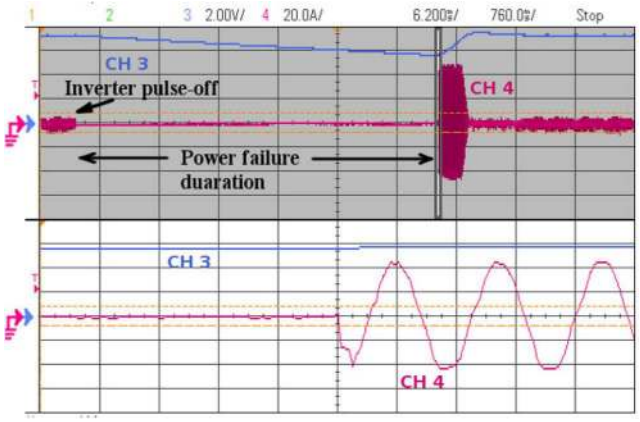

Fig. 22 *Speed and stator current waveforms during on-the-fly start with pulse-off method under no-load. Ch3: $\hat{\omega}_r$, Ch4: i_a (X-axis: 0.76 s/div; Y-axis: Ch3: 240 mech. rpm/div, Ch4: 20 A/div)*

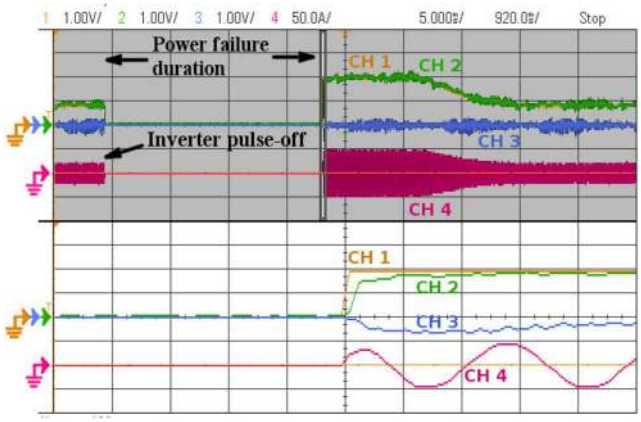

Fig. 23 *Variation of d-axis and q-axis currents during on-the-fly start with pulse-off method under loaded condition. Ch1: i_{q_ref}, Ch2: i'_q, Ch3: i'_d, Ch4: i_a (X-axis: 0.92 s/div; Y-axis: Ch1, Ch2, Ch3: 40 A/div, Ch4: 50 A/div)*

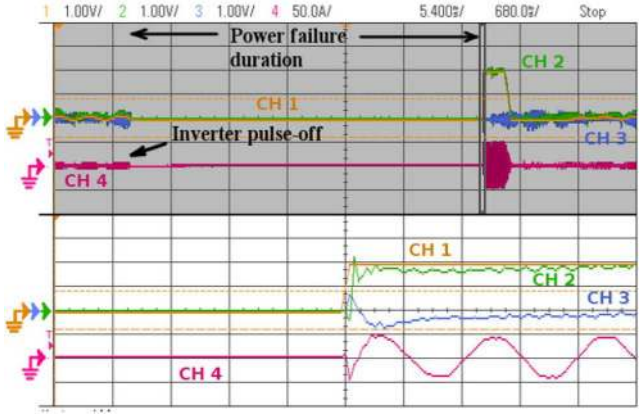

Fig. 24 *Variation of d-axis and q-axis currents during on-the-fly start with pulse-off method under no-load. Ch1: i_{q_ref}, Ch2: i'_q, Ch3: i'_d, Ch4: i_a (X-axis: 0.68 s/div; Y-axis: Ch1, Ch2, Ch3: 40 A/div, Ch4: 50 A/div)*

7 Conclusion

A quick and smooth changeover from I-f open-loop control to sensorless vector control is achieved using the proposed pulse-off method. The problems associated with the direct transition method is analysed in detail using simulation. Since the proposed method estimates the rotor position using line voltage sensors at zero current, the method is independent of machine parameters. Hence, the integrators of speed filter and speed controller are initialised with accurate speed and *q*-axis current demanded by the load, respectively, ensuring a smooth transition. The current decay time required by the method is derived analytically using the motor model. The small pulse-off duration will not cause a significant dip in rotor speed for high inertial machines. The proposed method is extended to perform a reliable and seamless on-the-fly start during short time power supply failure, without resorting to any complex algorithms. Furthermore, the line voltage sensors are also used to recalibrate the rotor flux linkage parameter in the pulse-off duration. Finally, the performance of the proposed method is validated on a 25 kW PMSM drive.

8 References

[1] Consoli, A., Scarcella, G., Testa, A.: 'Industry application of zero-speed sensorless control techniques for PM synchronous motors', *IEEE Trans. Ind. Appl.*, 2001, **37**, (2), pp. 513–521

[2] Corley, M.J., Lorenz, R.D.: 'Rotor position and velocity estimation for a salient-pole permanent magnet synchronous machine at standstill and high speeds', *IEEE Trans. Ind. Appl.*, 1998, **34**, (4), pp. 784–789

[3] Kim, H., Huh, K.K., Lorenz, R.D., *et al.*: 'A novel method for initial rotor position estimation for IPM synchronous machine drives', *IEEE Trans. Ind. Appl.*, 2004, **40**, (5), pp. 1369–1378

[4] Yun, S.Y., Lee, H.J., Lee, J.J., *et al.*: 'Research on the starting methods for initial driving of PMSM'. 2012 15th Int. Conf. on Electrical Machines and Systems (ICEMS), Sapporo, Japan, 2012, pp. 1–5

[5] Fatu, M., Teodorescu, R., Boldea, I., *et al.*: 'I-F starting method with smooth transition to EMF based motion-sensorless vector control of PM synchronous motor/generator'. 2008 IEEE Power Electronics Specialists Conf., Rhodes, Greece, 2008, pp. 1481–1487

[6] Baratieri, C.L., Pinheiro, H.: 'An I-F starting method for smooth and fast transition to sensorless control of BLDC motors'. 2013 Brazilian Power Electronics Conf., Gramado, Brazil, 2013, pp. 836–843

[7] Lu, K., Vetuschi, M., Rasmussen, P.O., *et al.*: 'Determination of high-frequency *d*- and *q*-axis inductances for surface-mounted permanent-magnet synchronous machines', *IEEE Trans. Instrum. Meas.*, 2010, **59**, (9), pp. 2376–2382

[8] Zhu, Z.Q., Li, Y., Howe, D., *et al.*: 'Influence of machine topology and cross-coupling magnetic saturation on rotor position estimation accuracy in extended back-emf based sensorless PM brushless ac drives'. 2007 IEEE Industry Applications Annual Meeting, New Orleans, USA., 2007, pp. 2378–2385

[9] Guglielmi, P., Pastorelli, M., Vagati, A.: 'Cross saturation effects in IPM motors and related impact on zero-speed sensorless control'. Fourtieth IAS Annual Meeting. Conf. Record of the 2005 Industry Applications Conf., 2005, Kowloon, Hong Kong, 2005, vol. 4, pp. 2546–2552

[10] Stirban, A., Boldea, I., Andreescu, G., *et al.*: 'Motion sensorless control of BLDC PM motor with offline FEM info assisted state observer'. 2010 12th Int. Conf. on Optimization of Electrical and Electronic Equipment, Brasov, Romania, 2010, pp. 321–328

[11] Wang, Z., Lu, K., Blaabjerg, F.: 'A simple startup strategy based on current regulation for back-EMF-based sensorless control of PMSM', *IEEE Trans. Power Electron.*, 2012, **27**, (8), pp. 3817–3825

[12] Kung, Y., Risfendra, , Lin, Y., *et al.*: 'FPGA-based sensorless controller for PMSM drives using sliding mode observer and phase locked loop'. 2016 Int. Conf. on Applied System Innovation (ICASI), Okinawa, Japan, 2016, pp. 1–4

[13] Kung, Y., Risfendra, : 'Modelsim/Simulink co-simulation of a sensorless control for PMSM drives based on I-F startup and EKF'. 2016 Int. Conf. on Applied System Innovation (ICASI), Okinawa, Japan, 2016, pp. 1–4

[14] Ortombina, L., Tinazzi, F., Zigliotto, M.: 'An effective start-up algorithm for sensorless synchronous reluctance and IPM motor drives'. 2017 IEEE 12th Int. Conf. on Power Electronics and Drive Systems (PEDS), Honolulu, USA., 2017, pp. 1062–1067

[15] Wang, W., Li, Z., Xu, X.: 'A novel smooth transition strategy for BEMF-based sensorless drive startup of PMSM'. Proc. 11th World Congress on Intelligent Control and Automation, Shenyang, People's Republic of China, 2014, pp. 4296–4301

[16] Wang, M., Xu, Y., Zou, J., *et al.*: 'An optimized I-F startup method for BEMF-based sensorless control of SPMSM'. 2017 IEEE Transportation Electrification Conf. and Expo, Asia-Pacific (ITEC Asia-Pacific), Harbin, People's Republic of China, 2017, pp. 1–6

[17] Zhang, Z., Guo, H., Liu, Y., *et al.*: 'An improved sensorless control strategy of ship IPMSM at full speed range', *IEEE Access*, 2019, **7**, pp. 178652–178661

[18] Niu, L., Zhai, J., Liu, X., *et al.*: 'A smooth and fast transition method for PMSM SMO based sensorless control'. 2016 IEEE 2nd Annual Southern Power Electronics Conf. (SPEC), Auckland, New Zealand, 2016, pp. 1–6

[19] Damodharan, P., Vasudevan, K.: 'Sensorless brushless dc motor drive based on the zero-crossing detection of back electromotive force (EMF) from the line voltage difference', *IEEE Trans. Energy Convers.*, 2010, **25**, (3), pp. 661–668

[20] Chen, H.-C., Liaw, C.-M.: 'Current-mode control for sensorless BDCM drive with intelligent commutation tuning', *IEEE Trans. Power Electron.*, 2002, **17**, (5), pp. 747–756

[21] Su, G.-J., McKeever, J.W.: 'Low-cost sensorless control of brushless dc motors with improved speed range', *IEEE Trans. Power Electron.*, 2004, **19**, (2), pp. 296–302

[22] Shen, J.X., Iwasaki, S.: 'Sensorless control of ultrahigh-speed PM brushless motor using PLL and third harmonic back EMF', *IEEE Trans. Ind. Electron.*, 2006, **53**, (2), pp. 421–428

[23] Son, Y.-C., Bae, B.-H., Sul, S.-K.: 'Sensorless operation of permanent magnet motor using direct voltage sensing circuit'. Conf. Record of the 2002 IEEE

Industry Applications Conf. 37th IAS Annual Meeting (Cat. No. 02CH37344), Pittsburgh, USA., 2002, vol. 3, pp. 1674–1678
[24] Batzel, T.D., Comanescu, M.: 'Instantaneous voltage measurement in PWM voltage source inverters'. 2007 Int. Aegean Conf. on Electrical Machines and Power Electronics, Bodrum, Turkey, 2007, pp. 168–173
[25] Wang, Y., Xu, Y., Niimura, N., *et al.*: 'Using volt-second sensing to directly improve torque accuracy and self-sensing at low speeds', *IEEE Trans. Ind. Appl.*, 2017, **53**, (5), pp. 4472–4482
[26] Schubert, M., De Doncker, R.W.: 'Instantaneous phase voltage sensing in PWM voltage-source inverters', *IEEE Trans. Power Electron.*, 2018, **33**, (8), pp. 6926–6935
[27] Nair, S.V., Hatua, K., Prasad, N.V.P.R.D., *et al.*: 'Pulse turn-off method for starting of PMSM drive using back-EMF position estimation technique'. 2017 IEEE Transportation Electrification Conf. (ITEC-India), Pune, India, 2017, pp. 1–6
[28] Wu, C., Zhao, Y., Sun, M.: 'Enhancing low-speed sensorless control of PMSM using phase voltage measurements and online multiple parameter identification', *IEEE Trans. Power Electron.*, 2020, **35**, (10), pp. 10700–10710
[29] Wu, T., Luo, D., Huang, S., *et al.*: 'A fast estimation of initial rotor position for low-speed free-running IPMSM', *IEEE Trans. Power Electron.*, 2020, **35**, (7), pp. 7664–7673
[30] Pravica, L., Sumina, D., Barisa, T., *et al.*: 'Flying start of a permanent magnet wind power generator based on a discontinuous converter operation mode and a phase-locked loop', *IEEE Trans. Ind. Electron.*, 2018, **65**, (2), pp. 1097–1106
[31] Jukic, F., Pravica, L., Barisa, T., *et al.*: 'Flying-start and continuous operation of a permanent-magnet wind generator based on discontinuous currents, discrete second-order sliding-mode observer and phase-locked loop', *IET Renew. Power Gener.*, 2020, **14**, (1), pp. 90–99
[32] Nair, S.V., Hatua, K., Durga Prasad, N., *et al.*: 'A smooth and stable open-loop I-F control for a surface mount PMSM drive by ensuring controlled starting torque'. IECON 2018 – 44th Annual Conf. of the IEEE Industrial Electronics Society, Washington DC, USA., 2018, pp. 355–360
[33] Kan, K.S., Tzou, Y.Y.: 'A sensorless I/f control method for single-phase BLDC fan motors with efficiency optimization by power factor control'. Proc. 7th Int. Power Electronics and Motion Control Conf., Harbin, People's Republic of China, 2012, vol. 4, pp. 2537–2541
[34] Boldea, I., Moldovan, A., Tutelea, L.: 'Scalar V/f and I-f control of AC motor drives: an overview'. 2015 Int. Aegean Conf. on Electrical Machines Power Electronics (ACEMP), 2015 Int. Conf. on Optimization of Electrical Electronic Equipment (OPTIM), 2015 Int. Symp. on Advanced Electromechanical Motion Systems (ELECTROMOTION), Side, Turkey, 2015, pp. 8–17
[35] Perera, P.D.C., Blaabjerg, F., Pedersen, J.K., *et al.*: 'A sensorless, stable V/f control method for permanent-magnet synchronous motor drives', *IEEE Trans. Ind. Appl.*, 2003, **39**, (3), pp. 783–791
[36] Borisavljevic, A., Polinder, H., Ferreira, J.A.: 'Realization of the I/f control method for a high-speed permanent magnet motor'. The XIX Int. Conf. on Electrical Machines – ICEM 2010, Rome, Italy, 2010, pp. 1–6
[37] Haichao, F., Boyang, S., Lizhen, G.: 'A closed-loop I/f vector control for permanent magnet synchronous motor'. 2017 9th Int. Conf. on Modelling, Identification and Control (ICMIC), Kunming, Yunnan, China, 2017, pp. 965–969
[38] Hurst, K.D., Habetler, T.G., Griva, G., *et al.*: 'Zero-speed tacho-less IM torque control: simply a matter of stator voltage integration', *IEEE Trans. Ind. Appl.*, 1998, **34**, (4), pp. 790–795
[39] Jahns, T.M., Soong, W.L.: 'Pulsating torque minimization techniques for permanent magnet ac motor drives – a review', *IEEE Trans. Ind. Electron.*, 1996, **43**, (2), pp. 321–330